


Traditional Semiconductors in the Two-Dimensional Limit

Michael C. Lucking, Weiyu Xie, Duk-Hyun Choe, Damien West,* Toh-Ming Lu, and S. B. Zhang
Department of Physics, Applied Physics & Astronomy, Rensselaer Polytechnic Institute, Troy, New York 12180, USA

 (Received 24 April 2017; published 23 February 2018)

Interest in two-dimensional materials has exploded in recent years. Not only are they studied due to their novel electronic properties, such as the emergent Dirac fermion in graphene, but also as a new paradigm in which stacking layers of distinct two-dimensional materials may enable different functionality or devices. Here, through first-principles theory, we reveal a large new class of two-dimensional materials which are derived from traditional III-V, II-VI, and I-VII semiconductors. It is found that in the ultrathin limit the great majority of traditional binary semiconductors studied (a series of 28 semiconductors) are not only kinetically stable in a two-dimensional double layer honeycomb structure, but more energetically stable than the truncated wurtzite or zinc-blende structures associated with three dimensional bulk. These findings both greatly increase the landscape of two-dimensional materials and also demonstrate that in the double layer honeycomb form, even ordinary semiconductors, such as GaAs, can exhibit exotic topological properties.

DOI: [10.1103/PhysRevLett.120.086101](https://doi.org/10.1103/PhysRevLett.120.086101)

Most known two-dimensional (2D) materials are derivatives of layered three-dimensional (3D) materials. From a coordination chemistry viewpoint, however, the crystal structure of any 2D system, or thin film, need not be that of bulk. For example, atomic-layer-thin semiconductors exist in the single-layer honeycomb (SLHC) structure such as graphene, silicene, and germanene [1–5] with variable stability. Are these merely happenstances, or do they suggest a universal trend that *all* bulk materials could be synthesized in some form of layered structure? Recent experiment suggests that this may indeed be the case [6], where by using a bilayer graphene as a capping layer, one can grow GaN, a traditional wide-gap 3D semiconductor, into a bilayer on a SiC substrate. This opens the door for engineering layered structures from conventional binary semiconductors. Additionally, there have been theoretical indications, in which first-principles calculations have shown that at least a handful of the binary semiconductors such as GaN and ZnO are stable in the SLHC form, as judged by the lack of imaginary phonon frequencies [1,2,7,8]. However, unlike graphene but similar to silicene and germanene, these artificial 2D semiconductors usually buckle due to the chemical difference between *A* and *B* elements.

Study of 2D materials has been intense, fueled by the realization of novel properties and quantum physics at confined dimensions. Graphene, for example, exhibits an unusual relativistic Dirac fermion behavior at the Fermi level, giving rise to exceptionally large carrier mobility. Silicene and germanene, while maintaining certain advantages of graphene, offer enhanced spin-orbit coupling (SOC). Hexagonal boron nitride (*h*-BN) is, on the other hand, a 2D insulator, which can be used to support and separate other 2D materials [9]. While SLHCs, other than

h-BN, are yet to be synthesized, first-principles calculations suggested that they are semiconductors with a band gap typically larger than bulk, in startling contrast to other emerging 2D semiconductors, e.g., transition metal dichalcogenides that exhibit intervalley coupling [10–13], and 2D metals, e.g., unit-cell-layer-thick metallic FeSe films on strontium titanate, which exhibit high-temperature superconductivity at a $T_C = 109$ K [14].

In this Letter, we show by first-principles calculations that many traditional 3D semiconductors can exist in stable layered forms with structures that are distinct from their three dimensional counterparts. By surveying binary semiconductors, we find that in the ultrathin limit, the most stable form of II-VI and III-V semiconductors are neither that of truncated bulk nor the SLHC structure, but instead we find that bulk truncated in the (111) direction (TB) tends to spontaneously relax to a double-layer honeycomb (DLHC) structure where individual SLHCs are bound together by dative bonds. The DLHC structure is not only kinetically stable, but also more energetically stable than either SLHC or TB as one approaches the ultrathin limit. Although weaker than a covalent bond, the doubling of the bond density and an elimination of chemically reactive cation dangling bonds make the DLHC more stable than TB. Additionally, multiple-layer DLHCs can also form with pure van der Waals (vdW) interaction between layers. A fascinating property of the DLHC structure is that the parity of the conduction band alternates with increasing number of layers. In the case of InSb, InAs, GaSb, GaAs, and HgTe, this leads to a unique type of topological behavior, a vdW interaction induced normal (NI) to topological (TI) insulator transition. Further, the large exciton binding in these 2D semiconductors, coupled with instances of a vanishing band gap suggest a path towards

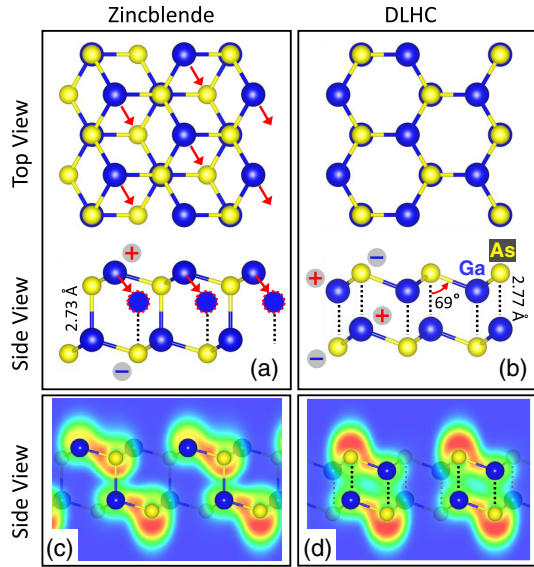


FIG. 1. (a) Top and side views of bilayer-thick TB and (b) DLHC GaAs. Red arrows in (a) indicate atomic displacements to form DLHC from TB. Charged atoms are denoted schematically by the (+) and (−) signs. (c),(d) The corresponding ELF maps with contour values ranging from 0 (blue) to 0.8 (red).

the realization of an excitonic insulator, which has been elusive in 3D systems.

Previous studies have shown that a number of binary semiconductors can exist as SLHC, often when either *A* or *B* is a first-row element (e.g., B, N, or O) [1,2]. While experiment shows the formation of a double layer for nitrides [6], this seems to be due to strong interaction with the substrate. As discussed by previous authors [2,7], first-row elements seem to form very flat structures (as opposed to the staggered bonding associated with DLHC) which suggests the stabilization of the SLHC structure for binaries consisting of these elements. A large number of conventional semiconductors are, however, unstable in the SLHC structure, as evidenced by their imaginary phonon frequencies [1,2,7]. However, here we find that two unstable SLHCs can bind spontaneously to form a stable DLHC, which can be viewed as transforming two-monolayer thick TB by displacing the topmost-cation layer relative to the remainder of the slab [see, e.g., Fig. 1(a) for GaAs] [5]. In a way, the transformation “hides” surface cations by doubling the number of interlayer bonds, as indicated by the dashed lines in Fig. 1(a). By symmetry, all interlayer bonds in DLHC are identical [see Fig. 1(b)]. However, the interlayer bonding that stabilizes the DLHC is qualitatively different from the original *AB* bonds, as revealed by the electron localization function (ELF) in Figs. 1(c) and 1(d). The ELF for DLHC shows significantly less electron localization in the interlayer region, indicating that the interlayer binding of DLHC is more ionic in nature. This is also reflected in the bond angle of 69° which is far from the ideal tetrahedral bond angle of 109.47° . By comparing

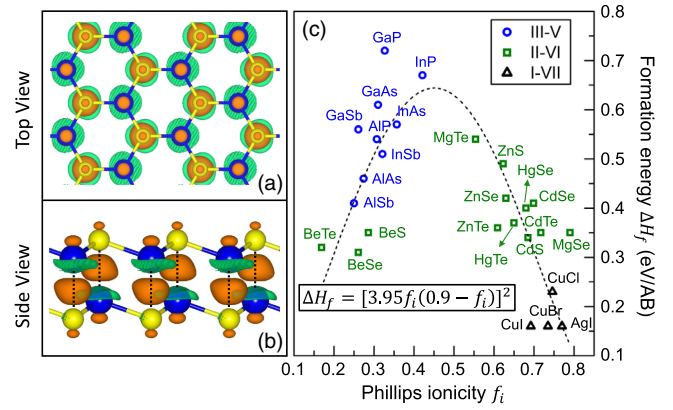


FIG. 2. Charge density difference between DLHC and SLHCs for GaAs in (a) top and (b) side view, respectively. The displayed isosurface value is $3 \times 10^{-3} e/\text{\AA}^3$ with the light brown being positive and green being negative. (c) Formation energy per formula unit of the calculated DLHCs (relative to infinite periodic bulk) as a function of Phillips ionicity. The dotted line is a two parameter least-squares fit to the data.

DLHC with two isolated SLHCs, the difference in charge density $\Delta\rho$ of which is shown in Figs. 2(a) and 2(b), we find charge is transferred across the interface from Ga to As. This is accompanied with a binding energy of $1.0 \text{ eV}/(1 \times 1)$ calculated via hybrid functional + SOC + D3 vdW interactions (HSD) [15–20], as detailed in the Supplemental Material [21]. While this value is only a third of the standard Ga-As bonding strength of $3 \text{ eV}/(1 \times 1)$, it is 3 times that of the interlayer vdW energy. This type of binding is characteristic of level repulsion between the high-lying empty state of cation and the low-lying doubly occupied state of anion [22], as schematically depicted in Fig. S1a in the Supplemental Material [21]. The repulsion lowers system total energy by lowering the energy of occupied states.

The stability of the interlayer bonding is reflected in the formation energies, ΔH_f , with respect to bulk and the phonon dispersions, which are presented for each of the 28 DLHCs in Table S1 and Fig. S2, respectively. Figure 2(c) shows a systematic trend between ΔH_f and Phillips ionicity f_i [23], where a least-squares fit yields $\Delta H_f = [3.95f_i(0.9 - f_i)]^2$. The approximate dome shape may reflect the competition between dipole repulsion in Fig. 1(b), which increases with f_i , and the stability of lone pairs, which also increases with f_i . While charge transfer between cation and anion is essential to satisfy the electron counting model (ECM) [24], the resulting dipoles are heads on, due to the central symmetry of the DLHC, and are hence repulsive. As the ionicity becomes increasingly large, see the structures of HgSe and AgI in Fig. S3 of the Supplemental Material [21], the DLHC structure distorts slightly to decrease the coulombic energy by shortening the anion-cation interlayer distance relative to the cation-cation distance.

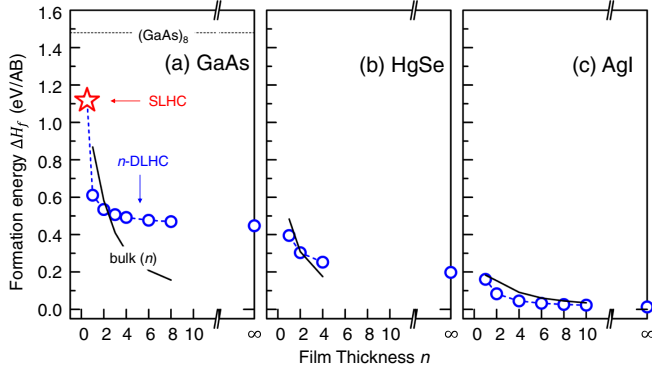


FIG. 3. Formation energies of DLHCs (open circles) and TBs (solid lines) as a function of layer thickness for (a) GaAs, (b) HgSe, and (c) AgI. The thickness n corresponds to the number of stacked DLHCs and is 4 times the number of atomic layers. In (a), the formation energy of SLHC and a $(\text{GaAs})_8$ cluster is also shown.

In addition to the ultra-thin limit of a single DLHC, there is a region of stability where DLHCs can be stacked to form a layered material. Figure 3 shows ΔH_f as a function of layer thickness n for III-V (GaAs), II-VI (HgSe), and I-VII (AgI), respectively. Unlike the formation of DLHC from the bonding between two SLHCs, here the chemically inert DLHCs are held together by vdW forces. Taking GaAs as an example, the binding energy $\Delta E = E(n+1) - [E(n) + E(\text{DLHC})] = 0.35 \text{ eV}/(1 \times 1)$ is quite insensitive to the number of layers, n . This binding can be directly traced back to the D3 vdW correction in the system Hamiltonian, which when turned “off” yields essentially zero binding between DLHC layers. This weak vdW binding results in large interlayer spacing between stacked DLHCs, the structure of which is shown for GaAs, HgSe, and AgI in Fig. S3 of the Supplemental Material [21].

As a result, the relative stability of the DLHC layered structure and TB form a universal trend. Namely, while the formation energy of the DLHC layered structure is largely independent of the number of layers, n , the TB shows a $1/r$ energy dependence which approaches that of bulk for large n . While the bulk ZB or WZ is lower in energy than that of bulk DLHC, the surface dangling bonds of the stable bulk form become energetically costly at small n [25]. Hence, there is a crossover in the stability between the bulk phase and the DLHC phase, with the DLHC being more stable for fewer numbers of layers, shown in Fig. 3. A more thorough comparison is given in Table S2 of the Supplemental Material [21], where the relative formation energy, $\delta(\Delta H_f) = \Delta H_f(n\text{DLHC}) - \Delta H_f(n\text{ bilayer TB})$, is tabulated for the 28 semiconductors. Here it can be seen all $n = 2$ DLHCs are more stable than TB, with the sole exception of CuCl. As n increases, III-V DLHCs become unstable first, followed by II-VI, and then by I-VII, DLHCs. At $n = 4$, only two III-V DLHCs, AlAs and AlSb, are stable. At $n = 8$, one II-VI DLHC, MgTe, is stable. At $n = 10$, however, two I-VII DLHCs, CuI and

AgI, remain to be stable. This result is in line with the report of AIP and AlN [5]. The kinetic stability of DLHC, along with the energetic stability relative to TB offer great hope that the manufacture of these 2D materials will someday be commonplace. One may consider laser thinning of a thicker film, the use of a vdW substrate, or a vdW cover as in Ref. [6]. Not only are most of the DLHCs more stable than silicene ($\Delta H_f = 1.45 \text{ eV}/\text{Si}_2$), which has been successfully experimentally fabricated by using a metal substrate; we note that they can even be more stable than 3D clusters. Taking GaAs in Fig. 3(a) as an example, ΔH_f is 1.48 eV per GaAs for a stoichiometric 8 GaAs cluster [26], which is even higher than the unstable SLHC.

Shifting focus from the stability of the DLHCs to their electronic properties, we find that most II-VI and I-VII DLHCs have a larger-than-bulk band gap, in line with the expectation from quantum confinement. Surprisingly, however, most III-V DLHCs have a smaller-than-bulk band gap. Detailed PBE results are given in Table S3 of Ref. [21]. From our earlier discussion (Fig. S1, Supplemental Material [21]), level repulsion is expected to push the valence band states down, while pushing the conduction band state up, thereby further enlarging the band gap. This understanding is clearly at odds with the results obtained for many of the III-V DLHCs. In fact, in the extreme cases of InSb, InAs, GaSb, GaAs, and HgTe, the gap closes to such a degree that band inversion across the Fermi level occurs, as determined by HSD calculation.

To understand this, we compare the band structures of SLHC [Fig. 4(a)] and DLHC [Fig. 4(c)] for GaAs. We note that, in bringing together two SLHCs to form DLHC, the SLHC states in Fig. 4(a) become doubly degenerate because each level has two identical copies (one from SLHC_1 and one from SLHC_2 ; see Fig. S4 in the Supplemental Material [21]). The formation of the DLHC lifts this degeneracy. Although a splitting between fully occupied (or empty states) has little effect in lowering the system formation energy, it can greatly alter the band structure. If we denote the wave functions of the degenerate SLHC states by ψ_1 and ψ_2 , the degenerate eigenenergies by ϵ_{SL} , and the coupling by $\Delta (> 0)$, the splitting can be modeled by $H = \begin{pmatrix} \epsilon_{\text{SL}} & -\Delta \\ -\Delta & \epsilon_{\text{SL}} \end{pmatrix}$. The solutions are

$$\varphi_+ = \frac{1}{\sqrt{2}}(\psi_1 + \psi_2) \quad \text{and} \quad \varphi_- = \frac{1}{\sqrt{2}}(\psi_1 - \psi_2), \quad (1)$$

with well-defined wave function character (WC) χ_2 : when $\chi_2 = (+)$, $\varphi = \varphi_+$ is a bonding state; when $\chi_2 = (-)$, $\varphi = \varphi_-$ is an antibonding state. Since the SLHC states also have their own WC, denoted here as c_1 , the overall WC of the DLHC states is thus given by a direct product $c_2 = \chi_2 \otimes c_1$. Incidentally, DLHC also has a parity denoted here as $P_2 = +$ for even and $P_2 = -$ for odd. In our choice of atomic origin, $c_2 = P_2$. We find that c is a

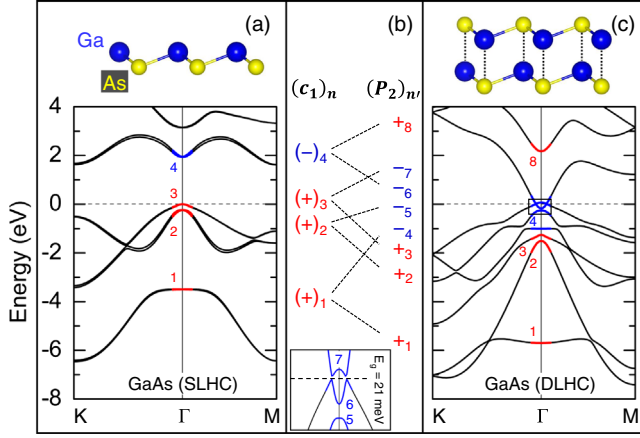


FIG. 4. Atomic and band structures of GaAs by HSD. (a) SLHC. (b) Character $(c_1)_n$ of the n th wave function of SLHC and parity $P_{n'}$ of the n' th wave function of DLHC at Γ (see main text for definition). (c) DLHC. Inset at the bottom of (b) is an enlargement of the framed area in (c) showing band inversion. Energy zero is at the valence band maximum.

much better descriptor than P , as c does not depend on the crystal symmetry.

Using the WC, we perform a mapping between the n th band in Fig. 4(a) and the n' th band in Fig. 4(c), as detailed in Fig. 4(b) (projection and identification of states is summarized in Fig. S5, Supplemental Material [21]). The results confirm unambiguously that level splitting is the origin for band inversion in DLHC GaAs. While such inversion is typically indicative of a TI, upon level splitting, the bonding state [$\chi_2 = (+)$] usually has a lower energy than the antibonding state [$\chi_2 = (-)$], the newly formed valence band maximum (VBM) should have $P_2 = \chi_2 c_1 = (+)(-) = -$ and the newly formed conduction band minimum (CBM) should have $P_2 = \chi_2 c_1 = (-)(+) = -$. The inversion thus happens between two states of the same parity, which does not affect the topological properties, so $Z_2 = 0$.

We note that going from SLHC to DLHC is a layer doubling process, and the resulting WC is $c_2 = \chi_2 \otimes c_1$. Going from DLHC to 2-DLHC is another layer doubling process which results in $c_4 = \chi_4 \otimes c_2$. Similar to the above discussion, in the formation of 2-DLHC, the degenerate VBM(CBM) associated with the single DLHC split again. This is shown in Fig. 5 for the case of GaAs. Here it can be seen that the band edges at Γ , both with $(-)$ parity, split into a higher lying $(-)$ state and a lower lying $(+)$ state. For the small gap of GaAs, this leads to the $(+)$ parity state (split off from the CBM) to cross with the $(-)$ parity state (split off from the VBM). As a result, band inversion between states with differing parity takes place when the two DLHCs are stacked. Direct calculation of the Z_2 invariant confirms this picture, with the 2-DLHC of GaAs becoming a topological insulator with $Z_2 = 1$. Note that we obtained qualitatively similar results, showing a non-trivial Z_2

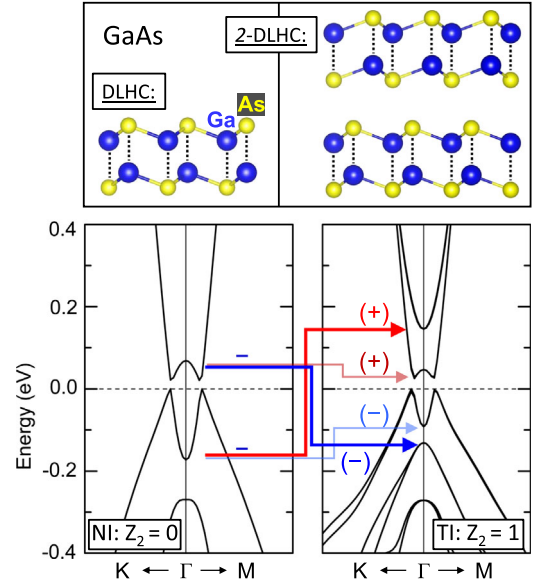


FIG. 5. Atomic and band structure of GaAs. Left is DLHC and right is 2-DLHC. In going from DLHC to 2-DLHC, splitting occurs in both the VBM and CBM. Both states, marked with $(-)$ parity, split into a higher lying $(-)$ state and a lower lying $(+)$ state. This leads to a second band inversion (indicated by the crossing between the thickened red and blue lines) which makes the GaAs 2-DLHC a TI.

invariant, using the highly accurate SCAN-rVV10 functional. This points toward a number of materials in addition to GaAs which are expected to yield a topological transition when going from DLHC to 2-DLHC: InSb, InAs, GaSb, and HgTe, all of which were found to have band inversion, albeit among states of the same parity. Note that the change of parity of the band edges also effect the optical transitions, irrespective of band inversion, as direct optical transitions at Γ become dipole allowed (Fig. S6, Supplemental Material [21]). Interestingly, it appears that SOC is not the deciding factor here for the observed topological properties; a similar conclusion was reached in our recent study of topological carbon [27] and transition metal dichalcogenides (TMDs) [28,29].

In addition to topological properties, our results suggest the DLHCs may be a good candidate for the formation of an excitonic insulator. Despite that the concept of an excitonic insulator was proposed half a century ago [30], its experimental realization in 3D materials has been elusive. 2D materials can be different: first, the exciton energy will increase by a factor of 4 due solely to a geometric effect [31]; second, owing to a reduction in dielectric screening at lower dimensions [32], the excitonic binding in 2D materials is expected further increase; e.g., it is nearly 20 times that of the 3D counterpart for MoS₂ [33]. While it is still a daunting challenge to calculate exciton energy by TDHF to meV accuracy, using this enhancement factor we can approximate the excitonic binding for DLHC HgTe as 18 meV

[34], which being larger than the band gap of 14 meV suggests that the ground state may be excitonic.

In summary, first-principles calculations point to a large new class of stable 2D materials derived from traditional semiconductors. This allows the traditional expertise of the semiconductor industry to be brought to bear on emerging technologies, such as 2D electronics and topological devices. Further, this work points to a new paradigm to discover a potentially new world of 2D layered materials out of traditionally 3D ones. While in the current case of traditional semiconductors, the recipe is to “bury or hide” chemically active cation sites inside the DLHC, the rule could vary in different class of solids and in different structures such as ZB, rocksalt, or perovskite. Even within the same structure class, results can be orientation dependent; e.g., one may build a 2D layered structure out of (001)-orientated semiconductor films. The electronic properties of the layered structures can be markedly different from those of 3D bulk, which is not only critically important for novel applications, but also a call for new physical understanding beyond traditional solid state theory.

M. L., W. Y. X., and T. M. L. were supported by the NSF Grant No. DMR-1305293, D. W. was supported by the NSF Grant No. EFMA-1542798, and D. H. C. and S. B. Z. were supported by the U.S. DOE Grant No. DESC0002623. The supercomputer time sponsored by NERSC under DOE Contract No. DE-AC02-05CH11231 and the CCI at RPI are also acknowledged.

M. C. L. and W. X. contributed equally to this work.

*Corresponding author.
damienwest@gmail.com

- [1] H. Zheng, X. B. Li, N. K. Chen, S. Y. Xie, W. Q. Tian, Y. Chen, H. Xia, S. B. Zhang, and H. B. Sun, *Phys. Rev. B* **92**, 115307 (2015).
- [2] H. L. Zhuang, A. K. Singh, and R. G. Hennig, *Phys. Rev. B* **87**, 165415 (2013).
- [3] A. K. Singh and R. G. Hennig, *Appl. Phys. Lett.* **105**, 042103 (2014).
- [4] C. L. Freeman, F. Claeysens, N. L. Allan, and J. H. Harding, *Phys. Rev. Lett.* **96**, 066102 (2006).
- [5] C. L. Freeman, F. Claeysens, N. L. Allan, and J. H. Harding, *J. Cryst. Growth* **294**, 111 (2006).
- [6] Z. Y. Al Balushi *et al.*, *Nat. Mater.* **15**, 1166 (2016).
- [7] H. Sahin, S. Cahangirov, M. Topsakal, E. Bekaroglu, E. Akturk, R. T. Senger, and S. Ciraci, *Phys. Rev. B* **80**, 155453 (2009).
- [8] S. Cahangirov, M. Topsakal, E. Akturk, H. Sahin, and S. Ciraci, *Phys. Rev. Lett.* **102**, 236804 (2009).
- [9] S. M. Kim *et al.*, *Nat. Commun.* **6**, 8662 (2015).
- [10] D. Xiao, G.-B. Liu, W. Feng, X. Xu, and W. Yao, *Phys. Rev. Lett.* **108**, 196802 (2012).
- [11] K. F. Mak, K. He, J. Shan, and T. F. Heinz, *Nat. Nanotechnol.* **7**, 494 (2012).
- [12] K. Behnia, *Nat. Nanotechnol.* **7**, 488 (2012).
- [13] H. Zeng, J. Dai, W. Yao, D. Xiao, and X. Cui, *Nat. Nanotechnol.* **7**, 490 (2012).
- [14] J.-F. Ge, Z.-L. Liu, C. Liu, C.-L. Gao, D. Qian, Qi-Kun Xue, Y. Liu, and J.-F. Jia, *Nat. Mater.* **14**, 285 (2015).
- [15] J. P. Perdew, K. Burke, and M. Ernzerhof, *Phys. Rev. Lett.* **77**, 3865 (1996).
- [16] G. Kresse and D. Joubert, *Phys. Rev. B* **59**, 1758 (1999).
- [17] G. Kresse and J. Furthmüller, *Comput. Mater. Sci.* **6**, 15 (1996).
- [18] S. Grimme, J. Antony, S. Ehrlich, and H. Krieg, *J. Chem. Phys.* **132**, 154104 (2010).
- [19] R. B. Capaz and Carsten A. Ullrich, *Braz. J. Phys.* **44**, 286 (2014).
- [20] A. A. Soluyanov and D. Vanderbilt, *Phys. Rev. B* **83**, 235401 (2011).
- [21] See Supplemental Material at <http://link.aps.org/supplemental/10.1103/PhysRevLett.120.086101> for details of the methodology and auxiliary figures, as well as tabulated results of the bandgaps, energetics, and phonon dispersions of each of the materials studied.
- [22] Y. Zhao, Y.-H. Kim, A. C. Dillon, M. J. Heben, and S. B. Zhang, *Phys. Rev. Lett.* **94**, 155504 (2005).
- [23] J. C. Phillips, *Bonds and Bands in Semiconductors* (Academic Press, New York, 1973).
- [24] M. D. Pashley, *Phys. Rev. B* **40**, 10481 (1989).
- [25] S. B. Zhang and S.-H. Wei, *Phys. Rev. Lett.* **92**, 086102 (2004).
- [26] Y. P. Feng, T. B. Boo, H. H. Kwong, C. K. Ong, V. Kumar, and Y. Kawazoe, *Phys. Rev. B* **76**, 045336 (2007).
- [27] Y. Chen, Y. Xie, S. A. Yang, H. Pan, F. Zhang, M. L. Cohen, and S. Zhang, *Nano Lett.* **15**, 6974 (2015).
- [28] D.-H. Choe, H.-J. Sung, and K. J. Chang, *Phys. Rev. B* **93**, 125109 (2016).
- [29] X. Qian, J. Liu, L. Fu, and J. Li, *Science* **346**, 1344 (2014).
- [30] D. Jérôme, T. M. Rice, and W. Kohn, *Phys. Rev.* **158**, 462 (1967).
- [31] S. V. Gaponenko, *Introduction to Nanophotonics* (Cambridge University Press, Cambridge, England, 2010).
- [32] L.-W. Wang and A. Zunger, *Phys. Rev. Lett.* **73**, 1039 (1994).
- [33] D. Y. Qiu, F. H. da Jornada, and S. G. Louie, *Phys. Rev. Lett.* **111**, 216805 (2013).
- [34] H. T. Grahn, *Introduction to Semiconductor Physics* (World Scientific, Singapore, 1999).